Manipulation of the Anoxic Metabolism in *Escherichia coli* by ArcB Deletion Variants in the ArcBA Two-Component System

Gonzalo N. Bidart,[a]† Jimena A. Ruiz,[b,c]† Alejandra de Almeida,[b] Beatriz S. Méndez,[b] and Pablo I. Nikel[a,b]#

Instituto de Investigaciones Biotecnológicas "Dr. Rodolfo A. Ugalde", Universidad Nacional de San Martín,[a] *Departamento de Química Biológica, Facultad de Ciencias Exactas y Naturales, Universidad de Buenos Aires, INQUIBICEN-CONICET,*[b] *and Instituto de Biociencias Agrícolas y Ambientales, CONICET,*[c] *Buenos Aires, Argentina*

Running headline: ArcB deletions and anoxic fluxome in *E. coli*

Section: Biotechnology

Keywords: *Escherichia coli*, ArcB, anoxic fluxome, redox balance, metabolic flux analysis, reduced biochemicals

---

Address correspondence to Pablo I. Nikel, Instituto de Investigaciones Biotecnológicas "Dr. Rodolfo A. Ugalde", Campus Miguelete UNSAM, Av. 25 de Mayo & Francia, 1650 Buenos Aires, Argentina. Phone: +54 11 4006 1500. Fax: +54 11 4724 1500. E-mail: pnikel@iib.unsam.edu.ar

† *Ex aequo* contribution

Bioprocesses conducted under conditions with restricted oxygen supply are increasingly exploited for the synthesis of reduced biochemicals using different biocatalysts. The model facultative anaerobe *Escherichia coli* has elaborate sensing and signal transduction mechanisms for redox control in response to the availability of O_2 and other electron acceptors. The ArcBA two-component system consists of ArcB, a membrane-associated sensor kinase, and ArcA, the cognate response regulator. The tripartite hybrid kinase ArcB possesses a transmembrane, a PAS, a primary transmitter (H1), a receiver (D1), and a phosphotransfer (H2) domain. Metabolic fluxes were compared under anoxic conditions in a wild-type *E. coli* strain, its Δ*arcB* derivative, and two partial *arcB* deletion mutants in which ArcB lacks either the H1 domain or the PAS-H1-D1 domains. These analysis revealed that elimination of different segments in ArcB determines a distinctive distribution of D-glucose catabolic fluxes, different from that observed in the Δ*arcB* background. Metabolite profiles, enzyme activity levels, and gene expression patterns were also investigated in these strains. Relevant alterations were observed at the *P-enol*-pyruvate/pyruvate and acetyl-coenzyme A metabolic nodes, and the formation of reduced fermentation metabolites such as succinate, D-lactate, and ethanol was favored in the mutant strains to different extents as compared to the wild-type strain. These phenotypic traits were associated to altered levels of the enzymatic activities operating at these nodes, as well as to elevated NADH/NAD^+ ratios. Thus, targeted modification of global regulators to obtain different metabolic flux distributions under anoxic conditions emerges as an attractive tool for metabolic engineering purposes.

INTRODUCTION

Anoxic fermentation of different carbon sources by *Escherichia coli* is increasingly gaining momentum in biotechnological setups aimed at obtaining reduced biochemicals. Relevant examples in this sense include (but are not limited to) the production of ethanol (47, 57), succinate (52), D-lactate (35), and polyhydroxyalkanoates (30); often using redox and/or regulatory *E. coli* mutants as the biocatalyst. These metabolic engineering approaches clearly underscore the need of a complete understanding of cell

physiology and metabolic network operativity under anoxic growth conditions. Metabolic fluxes through the central carbon pathways constitute the backbone of cell metabolism and represent the *in vivo* reaction rates of cognate enzymatic steps (51). The observed fluxome is the phenotypic consequence of both gene transcription and translation, as well as enzymatic activity and the regulation exerted at the metabolite level (38). As such, fluxome analysis is a useful approach to undertake the description of phenotypes associated with mutations in global regulators and constitutes a helpful strategy to harness the full biotechnological potential of redox mutants.

In *E. coli*, the metabolic regulation in response to changes in O_2 availability is mainly orchestrated by the ArcBA (anoxic redox control) two-component system (1, 7, 26, 48), which is composed of ArcB, the tripartite membrane-associated sensor kinase, and ArcA, the cognate response regulator. The ArcB sensor has a small transmembrane domain comprising 16 amino-acid residues followed by a leucine zipper and a PAS domain, that connects the transmembrane domain to the catalytic domains. ArcB also possesses three catalytic domains (Fig. 1A): a primary transmitter domain (H1), containing a conserved His^{292}; a receiver domain (D1), containing a conserved Asp^{576}; and a phosphotransfer (secondary transmitter) domain (H2), containing a conserved His^{717} (18, 20, 21). ArcA phosphorylation takes place through a phosphorelay process comprising the activity of all three domains (24). Under micro-oxic conditions, ArcB undergoes auto-phosphorylation (39) followed by intramolecular phosphate transfer and transphosphorylation of ArcA (17, 27). ArcA~P modulates the expression of *ca*. 135 genes (43), mainly acting as a negative transcriptional regulator of genes encoding enzymes involved in oxic pathways, such as the major dehydrogenase enzymes of the tricarboxylic acid (TCA) cycle and the glyoxylate shunt (49). At the same time, genes encoding enzymes belonging to fermentation pathways become activated by ArcA~P under micro-oxic or anoxic conditions (26, 34, 40). Respiratory pathways are also affected by the ArcBA system, since expression of *cyoABCDE* and *cydAB* is repressed and activated by ArcA~P, respectively (26, 49).

Genome-wide patterns of gene expression proved helpful to understand the complex ArcBA-dependent transcriptional regulation (41, 43). Unfortunately, and due to the diverse regulatory mechanisms that operate both at the post-translational and enzymatic activity levels, it is sometimes difficult to directly infer

phenotypic traits in mutant strains from these analysis. In particular, the biochemical mechanism of this regulatory system has been deciphered *in vitro* (2, 18), yet little is known about the *in vivo* effects of different *arcB* mutations on the central metabolic pathways of *E. coli* under anoxic growth conditions. In this study, the phenotypic and metabolic effects of targeted *arcB* deletions on the central carbon metabolism of *E. coli* was systematically evaluated under anoxic growth conditions through the analysis of growth parameters and the pattern of fermentation metabolites. The information was integrated in an *in silico* stoichiometric model of the central catabolic pathways, and was further substantiated by studying the transcription pattern of selected genes as well as *in vitro* measurements of relevant enzymatic activities. Taken together, the results show an incremental impact of partial deletions in ArcB on the distribution of metabolic fluxes under anoxic growth conditions that can be traced to the redox state. Furthermore, the incremental differences observed in the redox homeostasis among the mutant strains appear attractive for biotechnological purposes.

MATERIALS AND METHODS

Bacterial strains, oligonucleotides, and plasmids. All *Escherichia coli* strains are listed in Table 1 along with oligonucleotides and plasmids used in this work.

DNA manipulations and mutant construction. Standard DNA procedures followed well established protocols (44) and specific recommendations from manufacturers. Different protein domains in ArcB were eliminated by using the λ-Red recombination technology (12) in wild-type *E. coli* K1060. *E. coli* GNB1061, GNB1062, and GNB1063 were generated using amplification products (*i.e.*, *FRT-aphA-FRT*) obtained by PCR with oligonucleotides ΔH1-F and ΔH1-R, ΔPAS-F and ΔD1-R, and Δ*arcB*-F and Δ*arcB*-R, respectively, and plasmid pKD4 as the template. A DNA fragment encompassing nucleotides 802 to 1560 of *arcB* was deleted in *E. coli* GNB1061, resulting in an ArcB derivative in which the entire H1 domain was removed (*i.e.*, $ArcB^{268-520}$). In *E. coli* GNB1062, the PAS, H1, and D1 domains (*i.e.*, $ArcB^{177-640}$), were eliminated by deletion of the DNA segment comprised between nucleotides 529 and 1920 of *arcB* (Fig. 1A). An *arcB* deletion mutant, termed *E. coli* GNB1063, was also constructed using the same methodology. Antibiotic resistant determinants were eliminated by FLP-mediated recombination using plasmid pCP20

(10). A suitable pairwise combination of the oligonucleotides *arcB1*-C-F, *arcB1*-C-R, *arcB2*-C-F, *arcB2*-C-R, PDH-C-F, PAS-C-R, H1-C-R, and D1-C-R (Table 1), followed by DNA sequencing of the corresponding amplicons, were used to confirm that the correct deletions were introduced into the *arcB* locus.

Growth media and culture conditions. All cultures were incubated at 37°C at the indicated rotary agitation. During mutant construction and inocula preparation, cells were grown in LB medium (44) under oxic conditions. Pre-cultures and working cultures were carried out under anoxic conditions in 100-ml bottles containing 90 ml of M9 minimal medium containing 3% (wt/vol) D-glucose as the sole carbon source and supplemented with 1 $g \cdot l^{-1}$ Na_2S as a reducing agent. Bottles were incubated with rotary shaking at 125 rpm to avoid cell sedimentation, and anoxic conditions were qualitatively checked by adding 50 $\mu g \cdot l^{-1}$ resazurin to the culture medium. Whenever needed, antibiotics were used at the following concentrations: ampicillin, 100 $\mu g \cdot ml^{-1}$; kanamycin, 50 $\mu g \cdot ml^{-1}$; and chloramphenicol, 30 $\mu g \cdot ml^{-1}$. The Dye phenotype of the strains, growing under oxic conditions on toluidine blue O agar medium, was evaluated as previously described (9, 42).

Analytical procedures. Biomass concentration was determined as the cell dry weight (CDW) fraction of washed pellets from valorated broth aliquots dried at 65°C to constant weight. Dried samples were allowed to cool and held *in vacuo* until weighed.

Extracellular metabolic products and residual D-glucose in culture supernatants were determined by HPLC (using a HPX-87H column; BioRad Labs., Hercules, CA) as previously described (13). In some experiments, H_2 evolution was measured by head-space gas chromatography using a column packed with a divinylbenzene porous polymer (HayeSep DB; HayeSeparations Inc., Bandera, TX) and a thermal conductivity detector in a Varian3000 gas chromatograph and a 4000MS ion trap mass spectrometer (Bruker Daltonik GmbH, Bremen, Germany).

The intracellular content of NADH, NADPH, NAD^+, and $NADP^+$ was estimated by using *in vitro* procedures based on rapid inactivation of the metabolism of growing cells followed by acid or alkaline extraction of

nucleotides. Nucleotide content was determined by means of spectrophotometric cycling assays with 3-(4,5-dimethylthiazol-2-yl)-2,5-diphenyltetrazolium bromide as the final electron acceptor (5, 31).

Metabolic flux analysis based on metabolic pathway balances. A metabolic network designed for anaerobic *E. coli* cells was drafted by including the biochemical reactions corresponding to the Embden-Meyerhof-Parnas pathway, biomass generation from D-glucose-6-*P*, and fermentation pathways from *P*-*enol*-pyruvate, pyruvate, and acetyl-CoA (Fig. 2). Fermentation stoichiometry was derived from metabolic pathway balances. Cell composition was assumed to be the same in all experimental strains, and it was derived from Neidhardt et al. (28). Time-averaged concentrations in batch cultures, in which the specific rates of synthesis vary between two successive sampling periods (t and $t + \Delta t$), were estimated based on the average cell density according to the procedure described by Aristidou et al. (4). This methodology provides a good estimate when the specific rate of synthesis and the specific growth rate are more or less constant during consecutive sampling points, conditions which are assumed to be met under balanced growth (55). Metabolic fluxes (in mmol $\cdot$ g^{-1} $\cdot$ h^{-1}) were calculated from time-averaged concentrations of secretion metabolites and carbon source, and represent the average of 4-5 independent sampling points about the mid-exponential growth phase (*i.e.*, within balanced growth). Calculations that span the entire fermentation period indicated that indeed the time dependency of the fluxes was smallest during this interval (data not shown). The metabolic matrix was constructed based on the law of mass conservation and on the pseudo-steady state hypothesis on the intracellular intermediate metabolites (32, 45, 53). This formulation resulted in a set of linear equations that can be expressed as a stoichiometric matrix **A** of dimension $m \times n$, which was in turn related to vectors for net accumulation, $\mathbf{r}(m \times 1)$, and for metabolic fluxes, $\mathbf{v}(n \times 1)$. Considering the 13 reactions of the metabolic network (Fig. 2), and based solely on the measured extracellular metabolites and pseudo-steady state hypothesis balances of the intracellular intermediate metabolites, **A** becomes a square matrix ($m = v = 13$). The number of degrees of freedom equals the number of variables that were actually measured to describe the system, or, in some cases, were derived from experimental measurements. Standard mathematical methods were applied for the resolution of $\mathbf{A} \cdot \mathbf{v} = \mathbf{r} = \mathbf{0}$, and all fluxes within the network were derived from these stoichiometric constraints. Carbon balances were calculated from all the experimental and *in-silico* calculated fluxes, as well as the specific rate of CO_2 evolution, and biomass synthesis.

Quantitative reverse transcription (RT)-PCR. Genes studied in this work and the oligonucleotides used to analyze their expression are listed in Table 1. Culture samples were centrifuged at 10,000×*g* for 5 min at 4°C, washed once in ice-cold 50 mM Tris·HCl buffer (pH = 7.5), and then pelleted by centrifugation under the same conditions before total RNA was isolated using a commercially available kit (TRIzol Max™ Bacterial RNA Isolation Kit; Life Technologies Corp., Grand Island, NY). qRT-PCR reactions were carried out in an Applied Biosystems 7900HT Fast Real-Time PCR System™ (Life Technologies Corp.) using the Promega Reverse Transcription System™ (Promega Corp., Madison, WI). In RT reactions, the reaction mixture (containing 1 μg of RNA in 60 μl reaction mixtures), was incubated for 10 min at room temperature, followed by 30 min at 50ºC for reverse transcription, 5 min at 94ºC, and 10 min at 65ºC for reverse transcriptase inactivation. Amplification controls (containing RNA but not reverse transcriptase) were included in each run. The first strand cDNA was diluted to 250 μl with nuclease-free H_2O and further diluted 10-fold as needed. Quantitative PCR reactions were carried out in 96-well plates; each well contained 20 μl of a reaction mixture consisting of 2 μl diluted cDNA, 2 μl pre-mixed primers (1.25 pmol · μl^{-1}), 10 μl SYBR Green™ PCR Master mix, and 6 μl nuclease-free H_2O. Reaction mixtures were incubated 2 min at 50ºC, 10 min at 94ºC (*Taq* DNA polymerase activation), followed by 40 cycles of 15 s at 94ºC (denaturation), and 1 min at 60ºC (annealing and extension). Each plate included amplification controls as well as samples without template. The comparative C_T (threshold cycle) method ($\Delta\Delta C_T$) was applied for relative quantification of gene expression, and *rrsA*, encoding the 16S subunit of ribosomal RNA, was used as the control gene.

Enzyme activity measurements. Cells were harvested at OD_{600} = 0.5-0.7 by centrifugation at 10,000×*g* for 15 min at 4°C, washed twice with ice-cold 50 mM Tris·HCl buffer (pH = 7.5) containing 20 mM KCl, 5 mM $MgSO_4$, 2 mM 1,4-dithio-D-threitol, and 0.1 mM EDTA; and finally resuspended in the same buffer (*ca*. 0.5 g wet cells in 1 ml of buffer solution). The resulting cell suspension was stored at –20°C for 3 h, thawed in an ice bath, and disrupted by sonication. Cell-free extracts were obtained by centrifugation at 15,000×*g* for 30 min and 4°C. Crude enzyme extracts were immediately used for determinations as well as to measure protein concentration by means of the Bradford method (6). Enzyme activities were assayed spectrophotometrically in a thermostated recording Beckman DU 650 spectrophotometer (Beckman Coulter Inc., Fullerton, CA). The components of the reaction mixture were pipetted into a cuvette of 1-cm light path,

and the reaction was initiated by adding the cell-free extract or the appropriate substrate to give a final volume of 1 ml. Standard *in vitro* protocols for pyruvate kinase (50), D-glucose-6-*P* 1-dehydrogenase (16), pyruvate-formate lyase (23), D-lactate dehydrogenase (8), succinate dehydrogenase (56), citrate synthase (14), alcohol dehydrogenase (25), and acetate kinase (15) were used to estimate the enzymatic activities at stake. The extinction coefficient at 340 nm used for NADH and NADPH was 6.22 mM^{-1} cm^{-1}, and 1 unit of the specific enzyme activity was defined as the amount of enzyme required to convert 1 μmol of the substrate into the specific product per minute per milligram of protein.

Statistical analysis. All reported experiments were independently repeated at least twice, and the mean values of the corresponding parameter ± standard deviation (and, in the case of metabolic flux analysis, 90% confidence intervals) are presented. Determination of statistical significance between multiple comparisons was assessed using analysis of variance (ANOVA, with α = 0.01 and 0.05) followed by a Bonferroni post-test using transformed data whenever necessary.

RESULTS

Evaluation of the Dye phenotype in *E. coli* strains expressing different ArcB variants. The Dye phenotype, *i.e.*, sensitivity to the redox dye toluidine blue O (3, 42), was analyzed as a coarse estimation of the phenotypic effects caused by the deletions implemented in *arcB*. To this end, cultures of *E. coli* K1060 (wild-type strain), GNB1061 ($ArcB^{268-520}$), GNB1062 ($ArcB^{177-640}$), and GNB1063 (Δ*arcB*) were spotted onto plates containing this dye and their growth was scored after overnight incubation (Fig. 1B). *E. coli* K1060 grew well on toluidine blue O plates, whereas the Δ*arcB* strain formed much smaller colonies. However, *E. coli* GNB1061 and GNB1062 differed noticeably in their ability to grow on this medium. While *E. coli* GNB1061 formed colonies somewhat bigger than those of the Δ*arcB* strain (yet smaller than those of the wild-type strain), *E. coli* GNB1062 exhibited a phenotype similar to that observed for the Δ*arcB* strain. These traits prompted us to further evaluate the metabolic properties in the mutants that caused the alterations in colony size.

***E. coli* strains expressing different ArcB variants exhibit incremental phenotypic features.** Growth kinetic parameters of the strains under study were next analyzed in anoxic batch cultures. All experiments were conducted in M9 minimal medium supplemented with 3% (wt/vol) D-glucose in the absence of O_2 as the ArcBA two-component system is known to be active under these culture conditions (7). Interestingly, biomass concentration obtained after 24 h of cultivation was lower for mutants expressing the ArcB variants in comparison with the wild-type strain (*i.e.*, 36% and 60% lower for *E. coli* GNB1061 and GNB1062, respectively; Table 2). We also observed a reduction in the specific growth rate (μ_{max}) of the mutant strains (*i.e.*, 21% and 53% for GNB1061 and GNB1062, respectively; $P < 0.05$). As expected, *E. coli* GNB1063 showed the highest reduction in both final biomass concentration and μ_{max} (*i.e.*, 72% and 68% lower, respectively, when compared to the wild-type strain; $P < 0.05$), which is much lower than that observed in the strains bearing ArcB variants.

Specific rates of D-glucose consumption and yields of biomass on D-glucose ($Y_{X/S}$) were also determined in these cultures. All strains carrying ArcB variants showed a reduction in both parameters that qualitatively correlates with the results obtained for the specific growth rate and final biomass concentration (Table 2). The more marked differences among the partial mutants were observed in *E. coli* GNB1062, which showed a 27% and 62% reduction in both the specific rate of D-glucose consumption and $Y_{X/S}$, respectively, when compared to *E. coli* K1060 ($P < 0.05$). On the other hand, the Δ*arcB* strain exhibited a 40% and 73% reduction in the specific rate of D-glucose consumption and $Y_{X/S}$, respectively, when compared to the wild-type strain ($P < 0.01$).

In order to evaluate the metabolic state of the cells, the concentration of key fermentation metabolites was analyzed in culture supernatants of *E. coli* K1060 and the *arcB* mutant strains growing during 24 h under anoxic conditions and the corresponding yields on the carbon substrate were calculated. Metabolites detected in all cultures were formate, D-lactate, succinate, ethanol, and acetate. Higher concentrations of metabolic products in which carbon atoms are more reduced than in D-glucose were observed in cultures of the *arcB* strains as compared to those of *E. coli* K1060. The most significant differences in terms of yields on D-glucose were observed in acetate and ethanol. The acetate yield on D-glucose in the wild-type strain reached 0.89 ± 0.07 mol · mol^{-1}. While *E. coli* GNB1061 had a similar acetate yield (0.91 ± 0.07 mol ·

255 mol^{-1}), *E. coli* GNB1062 and GNB1063 have significantly lower values for this parameter than the wild-type
256 strain (0.68 $\pm$ 0.05 and 0.59 $\pm$ 0.04 mol $\cdot$ mol^{-1}, respectively; $P < 0.01$). On the other hand, the yield of
257 ethanol (the most reduced metabolite) on D-glucose followed the opposite trend. While in *E. coli* K1060 it
258 reached 0.52 $\pm$ 0.02 mol $\cdot$ mol^{-1}, the values for *E. coli* GNB1061, GNB1062, and GNB1063 were,
259 respectively, 0.59 $\pm$ 0.01, 0.81 $\pm$ 0.04, and 0.89 $\pm$ 0.03 mol $\cdot$ mol^{-1}.
260
261 **The pattern of secreted fermentation metabolites correlates with differences in the redox state in**
262 **the *arcB* mutants.** As the fate of carbon atoms at the acetyl-CoA node seemed to be markedly different in
263 the strains analyzed, we next studied the ethanol/acetate molar ratios under anoxic growth conditions.
264 Given the difference in the oxidation state of carbon atoms in these fermentation products, their molar ratio
265 provides a good estimation of the redox state of the cell (32, 48). All *arcB* mutant strains showed
266 significantly higher ethanol/acetate ratios than that obtained for *E. coli* K1060 (Table 3), which offers a
267 strong indication of an altered redox metabolism in the mutants. Among the partial deletion strains studied,
268 *E. coli* GNB1062 had the highest ethanol/acetate ratio (*i.e.*, 40% higher than that of the wild-type strain).
269 Again, the Δ*arcB* strain was the most severely affected in terms of redox balance, as the observed
270 ethanol/acetate ratio was 53% higher than that of the wild-type strain. In order to further correlate the
271 synthesis of oxidized and reduced fermentation metabolites with the redox state, we measured the actual
272 cellular content of nicotinamide dinucleotides (Table 3). In full accordance with the ethanol/acetate ratios, a
273 significant bias towards higher NADH/NAD$^+$ ratios was observed in the *arcB* mutants. In particular, *E. coli*
274 GNB1062 and GNB1063 had similar NADH/NAD$^+$ ratios, which were 44% and 69% higher than that of the
275 wild-type strain, respectively. Importantly, the NAD$^+$ + NADH content of the cells remained almost constant
276 (*ca.* 6 μmol $\cdot$ g^{-1}) among the strains under study.
277
278 **Metabolic flux distribution in central catabolic pathways is differentially affected by the redox state**
279 **in the *arcB* mutants.** Metabolic flux analysis based on stoichiometric constraints constitutes a
280 straightforward way to visualize the operativity of the entire metabolic network in anaerobic *E. coli* cells (4,
281 45, 55). Under these growth conditions, the carbon source is mostly converted into fermentation products
282 and, to a lesser extent, into biomass (11, 28). We applied this methodology to study the distribution of
283 metabolic fluxes in the *arcB* deletion mutants derived from wild-type K1060, using extracellular fluxes and

specific rates of D-glucose consumption as input for a simplified stoichiometric model of central carbon catabolism (Fig. 2). The actual flux values were normalized to the specific rate of D-glucose consumption of each strain, allowing us to establish comparisons between different strains (Table 4). The values of the carbon balance for each set of fluxes was close to the unit, suggesting a balanced closure between the carbon source consumed by the cells and the formation of biomass, end fermentation products, and CO_2.

In agreement with the experimental $Y_{X/S}$ values (Table 2), the flux towards biomass (from D-glucose-6-*P*) was consistently lower in all mutant strains when compared to that of *E. coli* K1060 ($P < 0.05$). Fluxes through the Embden-Meyerhof-Parnas pathway up to *P-enol*-pyruvate (v_2 and v_3) were higher in the *arcB* mutants (in particular for *E. coli* GNB1062 and GNB1063) than in *E. coli* K1060. Significant differences were also observed in the fluxes at the *P-enol*-pyruvate/pyruvate and acetyl-CoA metabolic nodes (see below). The NADH-dependent conversion of *P-enol*-pyruvate into succinate through the reductive branch of the TCA cycle (lumped in a single flux in the stoichiometric model, v_5) had a significantly higher value in the *arcB* mutants than in the wild-type strain. The increment in this flux in the mutants with respect to the wild-type strain ranged between 1.5-fold in *E. coli* GNB1061 to 2.8-fold in *E. coli* GNB1063 ($P < 0.01$). Considering that several genes of the TCA cycle are regulated by the ArcBA system (37, 49), and as citrate is the first intermediate of this metabolic pathway, we also quantified its concentration as a coarse estimation of the TCA cycle operativity towards the oxidative branch. As expected for anoxic cultures, the oxidative activity of the TCA cycle was almost null. Citrate concentrations were 0.18 ± 0.01 and 0.37 ± 0.02 mM for *E. coli* GNB1061 and GNB1062, respectively, compared to <0.05 mM for the parental strain. In contrast, the citrate concentration in culture supernatants of the Δ*arcB* strain attained 0.69 ± 0.08 mM.

Pyruvate can be either converted into acetyl-CoA and formate through the activity of pyruvate-formate lyase (PflB), or transformed into D-lactate by the fermentative, NADH-dependent D-lactate dehydrogenase (LdhA) (11). Surprisingly, we detected a small but clearly discernible rate of pyruvate secretion (v_6) in the wild-type strain and *E. coli* GNB1061, which in both cases accounted for <2% of the specific rate of D-glucose consumption, probably implying a limited processing of this metabolic intermediate *via* PflB/LdhA under anoxic conditions. D-lactate synthesis was higher in all *arcB* strains, which is in good agreement with their unregulated redox state that favors NADH oxidation. In particular, the flux through LdhA (v_7) was the

highest for *E. coli* GNB1063, the Δ*arcB* strain; closely followed by that of *E. coli* GNB1062 and representing a 2.9- and 2.1-fold increase, respectively, to the same flux in the wild-type strain ($P < 0.01$). The rate of pyruvate conversion into acetyl-CoA was similar in all strains, though the corresponding PflB flux (v_8) was slightly higher in the *arcB* mutants when compared to that of *E. coli* K1060 ($P = 0.085$). Subsequent processing steps of formate from this reaction were also markedly different among the experimental strains. The evolution of H_2 in these cultures was measured as a direct estimation of the formate-hydrogen lyase activity, which converts formate in H_2 and CO_2 (11). Judging by the values of the v_{10} flux derived from these measurements, the formate-hydrogen lyase activity was the highest in the wild-type strain, and decreased significantly in all the mutant strains. The lowest v_{10} value was observed in *E. coli* GNB1062, and was 1.2-fold lower than the flux in the wild-type strain ($P < 0.05$).

As explained in the preceding sections, acetyl-CoA can be either converted into acetate or ethanol under anoxic conditions. In *E. coli* K1060, the rate of ethanol synthesis (v_{11}) represents a 65.9% of that for D-glucose uptake, whereas acetate formation (v_{12}) accounts for 82.1%. This distribution between acetate and ethanol reflects the need to reoxidize reducing equivalents formed through the Embden-Meyerhof-Parnas pathway in order to achieve both redox and carbon balances. In line with this rationale, ethanol synthesis was favored over acetate accumulation in the mutants ($P < 0.05$), which also corresponded qualitatively to the high ethanol/acetate and NADH/NAD^+ ratios measured in these strains (Table 3). Again, the more evident differences were observed in *E. coli* GNB1062 and GNB1063. As a quantitative estimation of the molar fraction of carbon diverted from acetyl-CoA towards acetate and ethanol (f), the corresponding split ratios were calculated as $f_{ethanol} = v_{11}/(v_{11} + v_{12})$ and $f_{acetate} = v_{12}/(v_{11} + v_{12})$. In *E. coli* K1060, the values for $f_{ethanol}$ and $f_{acetate}$ were 44.5 and 55.5; whereas in *E. coli* GNB1062 and GNB1063 the split ratios were 50.9 and 49.1, and 54.2 and 45.8, respectively. The acetyl-CoA split ratio for ethanol in *E. coli* GNB1061 was slightly higher than that obtained for the wild-type strain, but the difference was barely significant ($P = 0.072$).

Finally, the availability of reducing power was also deduced at the fluxome level by considering the overall molar NADH availability per equivalent of consumed D-glucose, *i.e.*, $f_{NADH/G} = (2v_5 + v_7 + 2v_{11})/v_0$. The experimental value obtained for this parameter in the wild-type strain was 1.45 ± 0.08, and the increment in

342 $f_{NADH/G}$ in the mutants ranged from 1.1-fold for *E. coli* GNB1061 to 1.4-fold for *E. coli* GNB1063, thus
343 confirming the *in vitro* measurements of nucleotide content.
344
345 **Transcriptional analysis and measurement of key enzymatic activities support the observed**
346 **differences at the fluxome level.** In order to study the incremental effects of these deletions on the cell
347 physiology at different regulatory levels, we next determined the transcriptional activity of relevant genes by
348 quantitative RT-PCR as well as the activities of selected enzymes which showed significant differences
349 using the metabolic flux analysis approach (Fig. 3) under the same growth conditions used for those
350 experiments. These two levels of regulation were investigated at key points in different metabolic blocks
351 within the proposed anoxic biochemical network (*i.e.*, Embden-Meyerhof-Parnas pathway, pentose
352 phosphate pathway, TCA cycle, and fermentation pathways) to provide a complete snapshot of the
353 metabolic landscape in each strain.
354
355 D-Glucose is split into glycolysis and pentose phosphate pathway at the D-glucose-6-*P* branching point
356 (Fig. 2). A slight but consistent increase in the expression of *pfkA* (encoding the glycolytic enzyme 6-
357 phosphofructokinase I) was observed for *E. coli* GNB1062 and GNB1063 ($P < 0.05$, Fig. 3A), thus
358 suggesting a higher activity through the initial steps in D-glucose catabolism in the mutant strains when
359 compared to *E. coli* K1060 and in good agreement with the experimental values of v_3. The activity of
360 pyruvate kinase (PykAF, that converts *P-enol*-pyruvate into pyruvate) was analyzed to estimate carbon
361 routing through the lower Embden-Meyerhof-Parnas pathway (Fig. 3B). No significant differences were
362 observed in the specific PykAF activity among the strains, which correlates well with the flux values through
363 v_4 (Table 4). In stark contrast, the activity of D-glucose-6-*P* 1-dehydrogenase (encoded by *zwf*, and the key
364 enzyme of the oxidative pentose phosphate pathway) was >74% lower in all the mutant strains when
365 compared to *E. coli* K1060 (Fig. 3B), demonstrating that the flux towards pentoses formation was very low
366 in these strains. Moreover, the enzymatic activity observed in the wild-type strain was <50% than that
367 observed in oxic cultures of *E. coli* (data not shown).
368
369 The next metabolic node studied was the pyruvate branching point. In accordance with the expected
370 transcriptional activation of *focA-pflB* by the ArcBA system during the oxic/micro-oxic transition (46), the

level of *pflB* mRNA in *E. coli* GNB1063 was 26% lower than that of *E. coli* K1060 ($P < 0.05$, Fig. 3A). The difference in this parameter for the other mutants and the wild-type strain resulted not significant. *In vitro* enzymatic activity of PflB demonstrated that this activity is indeed affected by the different *arcB* mutations tested (Fig. 3B). In particular, the PflB activity was 36% and 27% lower in *E. coli* GNB1062 and GNB1063, respectively, than that measured in *E. coli* K1060 ($P < 0.05$). The level of activity detected in *E. coli* GNB1061 and *E. coli* K1060 was very similar. To also evaluate the contribution of the pyruvate dehydrogenase complex in the flux conducive to acetyl-CoA formation, we measured the transcriptional activity of *aceE*, which encodes the E1 component of this enzymatic complex (Fig. 3A). While no differences were observed for *E. coli* GNB1061 as compared to the wild-type strain, the transcriptional level of *aceE* was incremented 2.4- and 3.6-fold in *E. coli* GNB1062 and GNB1063, respectively ($P < 0.01$). Even when it is known that pyruvate dehydrogenase could contribute to acetyl-CoA formation under micro-oxic conditions (22), no significant enzymatic activity was detected in cell-free extracts of any of the strains under study (data not shown).

Fermentation pathways that operate at the *P-enol*-pyruvate/pyruvate metabolic node also showed significant differences among the mutants. Both *ldhA* (encoding D-lactate dehydrogenase) and *frdA* (encoding one of the fumarate reductase subunits, the enzymatic complex that converts fumarate into succinate) were strongly upregulated in all *arcB* mutants (Fig. 3A), attaining mRNA levels >2-fold higher than those observed in *E. coli* K1060 ($P < 0.01$). In the Δ*arcB* mutant, *ldhA* expression peaked at *ca*. 6-fold higher than in the wild-type strain. In contrast, *frdA* expression was the highest in *E. coli* GNB1062 (4.5-fold increment, $P < 0.01$). LdhA activity followed the same trend as that observed at the transcriptional level, being higher in all *arcB* mutants when compared to *E. coli* K1060 ($P < 0.05$, Fig. 3B). However, at least at this level of regulation, no significant differences were observed among mutant strains. Total succinate dehydrogenase (Sdh) activity was also higher in the mutants as compared to *E. coli* K1060, and the highest activity was observed in *E. coli* GNB1062, in accordance with the transcriptional regulation results obtained by means of quantitative RT-PCR. The behavior in the strain expressing $ArcB^{177-640}$, quantitatively different from that observed in the Δ*arcB* mutant, might suggest a particular regulation pattern on the reductive branch of the TCA cycle in that context.

The *in vitro* activity of citrate synthase was also evaluated under anoxic conditions to substantiate the results of citrate synthesis discussed above. GltA activity was higher in *E. coli* GNB1062 and GNB1063 than in the wild-type strain and in *E. coli* GNB1061, qualitatively reproducing the results obtained by measuring the extracellular citrate concentration. Although some residual activity of the oxidative branch of the TCA cycle is present in the *arcB* backgrounds analyzed in this study under anoxic conditions, our results clearly show a much higher activity towards succinate formation (*i.e.*, reducing branch).

The regulation at the acetyl-CoA branching point was then assessed by measuring the expression of *adhE* and *ackA*, as well as the corresponding alcohol dehydrogenase and acetate kinase activities. A good correlation between transcriptional regulation and enzymatic activity was observed for *adhE*. Indeed, a significant increment in both parameters was observed in the mutant strains in comparison with wild-type K1060 ($P < 0.05$), which was even more evident for *E. coli* GNB1062 and GNB1063 as compared to *E. coli* GNB1061. In particular, *adhE* transcription levels attained the maximum fold change among all the genes evaluated, being *ca*. 8-fold higher in *E. coli* GNB1063 than in *E. coli* K1060. While in *E. coli* GNB1062 and GNB1063 the levels of *ackA* did not differ significantly from those in wild-type K1060, *ackA* expression had a *ca*. 2.9-fold increment in *E. coli* GNB1061 (Fig. 3A). However, these sharp differences at the transcriptional level did not translate into a similar pattern at the enzymatic activity level. Moreover, AckA activity was lower in all the *arcB* mutants than in *E. coli* K1060, which fits well with the observed fluxes through this pathway (Fig. 3B). Both AdhE and AckA showed a regulatory pattern that qualitatively correlated with the changes observed at the flux level, thus reflecting the crucial competence between the corresponding pathways at the acetyl-CoA branching point in terms of both precursors and reducing power availability.

Finally, the transcriptional level of *arcA* was also evaluated, and no significant differences were observed in its transcription level among the experimental strains. Although the mechanism whereby the ArcB variants determine phenotypic differences in the mutants cannot be directly concluded from the present results and remains to be exposed, the transcriptional analysis suggests that the pattern of regulation of *arcA* is not significantly affected by the deletions introduced in *arcB*.

DISCUSSION

Metabolic manipulations to enhance the synthesis of metabolic products include several approaches to increase the availability of substrates needed for its formation or to eliminate competing pathways, which sometimes leads to undesired phenotypes. An alternative strategy that has been scarcely exploited is the network-wide manipulation of metabolic fluxes by means of mutations in global regulators. In this sense, the modularity of the ArcB sensor of the ArcBA two-component system (19), a prototypal member of the bacterial global regulatory network in the model facultative anaerobe *E. coli*, represents an ideal model to explore this approach. The present study analyzed some of the complex genotype-phenotype relationships in mutants of this regulatory system under anoxic growth conditions, which also permits to foresee their potential applicability for the synthesis of reduced biochemicals.

The relative lack of knowledge on the cellular wiring of these regulatory networks under conditions relevant to both laboratory and industrial applications represents a significant hurdle that has to be overcome for the efficient design of industrial processes. A complete analysis of the cellular physiology in different *arcB* mutants is needed in order to understand (and take advantage of) the metabolic effects of *arcB* mutations *in vivo*. Metabolic and physiological variations resulting from different deletions in the global regulator ArcB were systematically analyzed by combined physiological, transcriptomic, and fluxome analysis. This combined approach is relevant since deletion of global regulatory genes were observed to affect the entire cellular and metabolic landscape in a rather difficult-to-predict fashion.

The Dye phenotype served as an *a priori* indication of differences at the metabolic level among the mutants. Indeed, the overall colony morphology under these growth conditions was in good agreement with the altered metabolic patterns observed in each strain; while *E. coli* GNB1062 showed a Dye phenotype compatible with that of the Δ*arcB* strain, *E. coli* GNB1061 presented an intermediate phenotype, somewhat closer to that of the wild-type strain. These morphological alterations are likely to arise from differences in the redox homeostasis, as previously suggested (3, 42). In line with this hypothesis, all the mutants had a high NADH/NAD^+ ratio and the most significant differences were observed in the NADH content, as the NAD^+ content did not show changes in the different strains. In close connection with this trait, the split of

458 the acetyl-CoA between ethanol and acetate was predictably affected by the redox state measured in each
459 strain (see below).
460
461 The regulatory pattern of some fluxes (also observed at both the transcriptional and enzymatic activity
462 levels) significantly departs from that reported for *arcA* mutants under conditions with restricted O_2 supply
463 (32, 59), thus evidencing that elimination of the entire *arcB* coding sequence (or sequences encoding
464 different ArcB domains) has a different effect on the cell physiology as compared to the absence of the
465 cognate response regulator. For instance, the high glycolytic fluxes observed in the mutants (especially in
466 *E. coli* GNB1062 and GNB1063) result in an elevated NADH generation rate that cells need to recycle to
467 efficiently continue D-glucose catabolism; therefore, anoxic fermentation pathways have to fulfill the
468 requirement for NADH regeneration under these culture conditions (11). Although the increase in NADH in
469 the mutants can be mostly attributed to the activity of the Embden-Meyerhof-Parnas pathway, it is worth
470 considering that it can also arise from either a high activity of the TCA cycle enzymes and/or a low activity
471 of the electron transfer chain. Our results from transcriptomic analysis as well as enzymatic activity
472 measurements support some residual contribution of the TCA cycle to the redox balance, and the
473 repression of *cyoABCDE* (that encodes cytochrome *o*) by the ArcBA system is well known (26, 54).
474 However, the activity of the oxidative branch of the TCA cycle under the experimental conditions explored
475 here is expected to be low, considering the inhibition exerted by the high $NADH/NAD^+$ ratios themselves on
476 both GltA and 2-ketoglutarate dehydrogenase activities (37, 58).
477
478 The pyruvate/acetyl-CoA branching points showed the most striking alterations among the mutant strains.
479 PflB is known to convert pyruvate into acetyl-CoA under conditions with restricted O_2 supply (1), but recent
480 studies suggest that some activity of the pyruvate dehydrogenase complex also contributes to anoxic
481 acetyl-CoA formation (22). Under the working conditions tested in this study, pyruvate produced during
482 glycolysis seems to be mainly processed by pyruvate-formate lyase to generate acetyl-CoA. Since the
483 activity of the pyruvate dehydrogenase complex (the other source of acetyl-CoA from pyruvate besides
484 PflB) is inhibited by NADH (22), and higher ethanol/acetate and $NADH/NAD^+$ redox ratios were detected in
485 all *arcB* strains compared to the wild-type strain, the flux through pyruvate dehydrogenase would contribute
486 to acetyl-CoA only marginally. In turn, the acetyl-CoA metabolic node, at which carbon atoms from D-

glucose catabolism can be either converted into an oxidized or a reduced fermentation metabolite (*i.e.*, acetate or ethanol, respectively), is of paramount interest for the synthesis of various heterologous metabolites of industrial interest. By evaluating the flux values conducing to ethanol and acetate, as well as the flux split ratios for these two metabolites, it can be seen that the synthesis of reduced biochemicals is favored in all the mutants.

At this point, it is relevant to consider that the actual phenotype of each strain (*i.e.*, the macroscopic distribution of metabolic fluxes and other phenotypic traits) is the final consequence of multiple (and very complex) regulatory processes that act hierarchically at different levels (38, 40). Several fine-tuning mechanisms for metabolic modulation, such as allosteric regulation of enzyme activity, might well operate differently in the strains analyzed. However, one can safely assume that the gross regulatory mechanisms, other than that exerted by the ArcBA system itself, are similar in the parental strain and its *arcB* derivatives. The mechanism underlying the phenotypic differences observed could lie beyond the known phosphorelay process described *in vitro* for the cellular signaling mediated by the ArcBA system (24, 27). The possibility that similar (or radically different) effects on central metabolism could be observed in partial-deletion mutants of genes encoding components of other signal transduction systems in *E. coli* is an exciting scenario that remains to be explored.

Different types of mutations in components of global regulatory systems, such as *arcA* and *creB* (29-31, 33), have been shown to influence both carbon and redox balances in *E. coli*, mainly under micro-oxic growth conditions. The results of the current study focus on the manipulation of global regulators as a relevant tool to modulate central metabolic fluxes under anoxic conditions and to harness reducing power availability for biotechnological purposes. The unregulated redox state of the mutant strains provides diverse metabolic backgrounds for the synthesis of reduced biochemicals both native to *E. coli*, such as ethanol, D-lactate, and succinate; and those resulting from heterologous pathways, such as poly(3-hydroxybutyrate). Moreover, the use of targeted deletions in the ArcB tripartite sensor protein enabled us to obtain increasing phenotypic effects that could be further exploited for the synthesis of reduced biochemicals, such as those mentioned above.

ACKNOWLEDGEMENTS

We wish to thank D. Georgellis and V. de Lorenzo for sharing materials and for inspiring discussions. We are also indebted to M. Julia Pettinari for her critical advice while drafting the manuscript. J.A.R., A.D.A, B.S.M., and P.I.N. are career investigators from Consejo Nacional de Investigaciones Científicas y Técnicas (CONICET, Argentina).

REFERENCES

1. **Alexeeva S, de Kort B, Sawers G, Hellingwerf KJ, Teixeira de Mattos MJ.** 2000. Effects of limited aeration and of the ArcAB system on intermediary pyruvate catabolism in *Escherichia coli*. J. Bacteriol. **182:**4934-4940.
2. **Alvarez AF, Georgellis D.** 2010. *In vitro* and *in vivo* analysis of the ArcB/A redox signaling pathway. Methods Enzymol. **471:**205-228.
3. **Alvarez AF, Malpica R, Contreras M, Escamilla E, Georgellis D.** 2010. Cytochrome *d* but not cytochrome *o* rescues the toluidine blue growth sensitivity of *arc* mutants of *Escherichia coli*. J. Bacteriol. **192:**391-399.
4. **Aristidou AA, San KY, Bennett GN.** 1999. Metabolic flux analysis of *Escherichia coli* expressing the *Bacillus subtilis* acetolactate synthase in batch and continuous cultures. Biotechnol. Bioeng. **63:**737-749.
5. **Bernofsky C, Swan M.** 1973. An improved cycling assay for nicotinamide adenine dinucleotide. Anal. Biochem. **53:**452-458.
6. **Bradford MM.** 1976. A rapid and sensitive method for the quantitation of microgram quantities of protein utilizing the principle of protein-dye binding. Anal. Biochem. **72:**248-254.
7. **Bueno E, Mesa S, Bedmar EJ, Richardson DJ, Delgado MJ.** 2012. Bacterial adaptation of respiration from oxic to microoxic and anoxic conditions: redox control. Antioxid. Redox Signal. **16:**819-852.
8. **Bunch PK, Mat-Jan F, Lee NA, Clark DP.** 1997. The *ldhA* gene encoding the fermentative lactate dehydrogenase of *Escherichia coli*. Microbiology **143:**187-195.

9. **Buxton RS, Drury LS.** 1983. Cloning and insertional inactivation of the *dye* (*sfrA*) gene, mutation of which affects sex factor F expression and dye sensitivity of *Escherichia coli* K-12. J. Bacteriol. **154:**1309-1314.
10. **Cherepanov PP, Wackernagel W.** 1995. Gene disruption in *Escherichia coli*: Tc^R and Km^R cassettes with the option of Flp-catalyzed excision of the antibiotic-resistance determinant. Gene **158:**9-14.
11. **Clark DP.** 1989. The fermentation pathways of *Escherichia coli*. FEMS Microbiol. Rev. **5:**223-234.
12. **Datsenko K, Wanner BL.** 2000. One-step inactivation of chromosomal genes in *Escherichia coli* K-12 using PCR products. Proc. Natl. Acad. Sci. USA **97:**6640-6645.
13. **de Almeida A, Giordano AM, Nikel PI, Pettinari MJ.** 2010. Effects of aeration on the synthesis of poly(3-hydroxybutyrate) from glycerol and glucose in recombinant *Escherichia coli*. Appl. Environ. Microbiol. **76:**2036-2040.
14. **Dixon GH, Kornberg HL.** 1959. Assay methods for key enzymes of the glyoxylate cycle. Biochem. J. **73:**3-10.
15. **Ferry JG.** 2011. Acetate kinase and phosphotransacetylase. Methods Enzymol. **494:**219-231.
16. **Fraenkel DG, Horecker BL.** 1964. Pathways of D-glucose metabolism in *Salmonella typhimurium*. A study of a mutant lacking phosphoglucose isomerase. J. Biol. Chem. **239:**2765-2771.
17. **Georgellis D, Kwon O, Lin ECC.** 2001. Quinones as the redox signal for the *arc* two-component system of bacteria. Science **292:**2314-2316.
18. **Georgellis D, Lynch AS, Lin ECC.** 1997. *In vitro* phosphorylation study of the *arc* two-component signal transduction system of *Escherichia coli*. J. Bacteriol. **179:**5429-5435.
19. **Green J, Paget MS.** 2004. Bacterial redox sensors. Nat. Rev. Microbiol. **2:**954-966.
20. **Iuchi S, Lin ECC.** 1992. Mutational analysis of signal transduction by ArcB, a membrane sensor protein responsible for anaerobic repression of operons involved in the central aerobic pathways in *Escherichia coli*. J. Bacteriol. **174:**3972-3980.
21. **Iuchi S, Lin ECC.** 1992. Purification and phosphorylation of the Arc regulatory components of *Escherichia coli*. J. Bacteriol. **174:**5617-5623.
22. **Kim Y, Ingram LO, Shanmugam KT.** 2008. Dihydrolipoamide dehydrogenase mutation alters the NADH sensitivity of pyruvate dehydrogenase complex of *Escherichia coli* K-12. J. Bacteriol. **190:**3851-3858.

574 23. **Knappe J, Blaschkowski HP, Gröbner P, Schmitt T.** 1974. Pyruvate formate-lyase of *Escherichia*
575 *coli*: the acetyl-enzyme intermediate. Eur. J. Biochem. **50:**253-263.
576 24. **Kwon O, Georgellis D, Lin ECC.** 2000. Phosphorelay as the sole physiological route of signal
577 transmission by the arc two-component system of *Escherichia coli*. J. Bacteriol. **182:**3858-3862.
578 25. **Leonardo MR, Dailly Y, Clark DP.** 1996. Role of NAD in regulating the *adhE* gene of *Escherichia coli*.
579 J. Bacteriol. **178:**6013-6018.
580 26. **Lynch AS, Lin ECC.** 1996. Responses to molecular oxygen, p 1526-1538. *In* Neidhardt FC, Curtiss
581 3rd R, Ingraham JL, Lin ECC, Low KB, Magasanik B, Reznikoff WS, Riley M, Schaechter M, and
582 Umbarger HE (ed), *Escherichia coli* and *Salmonella*: cellular and molecular biology, 2nd ed, vol. 1.
583 ASM Press, Washington, D.C.
584 27. **Malpica R, Sandoval GR, Rodríguez C, Franco B, Georgellis D.** 2006. Signaling by the *arc* two-
585 component system provides a link between the redox state of the quinone pool and gene expression.
586 Antioxid. Redox Signal. **8:**781-795.
587 28. **Neidhardt FC, Ingraham JL, Schaechter M.** 1990. Physiology of the bacterial cell: a molecular
588 approach. Sinauer Associates, Sunderland, MA.
589 29. **Nikel PI, de Almeida A, Pettinari MJ, Méndez BS.** 2008. The legacy of HfrH: mutations in the two-
590 component system CreBC are responsible for the unusual phenotype of an *Escherichia coli arcA*
591 mutant. J. Bacteriol. **190:**3404-3407.
592 30. **Nikel PI, Pettinari MJ, Galvagno MA, Méndez BS.** 2008. Poly(3-hydroxybutyrate) synthesis from
593 glycerol by a recombinant *Escherichia coli arcA* mutant in fed-batch microaerobic cultures. Appl.
594 Microbiol. Biotechnol. **77:**1337-1343.
595 31. **Nikel PI, Pettinari MJ, Ramirez MC, Galvagno MA, Méndez BS.** 2008. *Escherichia coli arcA* mutants:
596 metabolic profile characterization of microaerobic cultures using glycerol as a carbon source. J. Mol.
597 Microbiol. Biotechnol. **15:**48-54.
598 32. **Nikel PI, Zhu J, San KY, Méndez BS, Bennett GN.** 2009. Metabolic flux analysis of *Escherichia coli*
599 *creB* and *arcA* mutants reveals shared control of carbon catabolism under microaerobic growth
600 conditions. J. Bacteriol. **191:**5538-5548.
601 33. **Nizam SA, Shimizu K.** 2008. Effects of *arcA* and *arcB* genes knockout on the metabolism in
602 *Escherichia coli* under anaerobic and microaerobic conditions. Biochem. Eng. J. **42:**229-236.

34. **Nizam SA, Zhu J, Ho PY, Shimizu K.** 2009. Effects of *arcA* and *arcB* genes knockout on the metabolism in *Escherichia coli* under aerobic condition. Biochem. Eng. J. **44:**240-250.
35. **Okano K, Tanaka T, Ogino C, Fukuda H, Kondo A.** 2010. Biotechnological production of enantiomeric pure lactic acid from renewable resources: recent achievements, perspectives, and limits. Appl. Microbiol. Biotechnol. **85:**413-423.
36. **Overath P, Schairer HU, Stoffel W.** 1970. Correlation of *in vivo* and *in vitro* phase transitions of membrane lipids in *Escherichia coli*. Proc. Natl. Acad. Sci. USA **67:**606-612.
37. **Park SJ, McCabe J, Turna J, Gunsalus RP.** 1994. Regulation of the citrate synthase (*gltA*) gene of *Escherichia coli* in response to anaerobiosis and carbon supply: role of the *arcA* gene product. J. Bacteriol. **176:**5086-5092.
38. **Patil KR, Bapat PM, Nielsen J.** 2010. Structure and flux analysis of metabolic networks, p 17.11-17.18. *In* Smolke CD (ed), The metabolic pathway engineering book - Fundamentals, 1st ed, vol. 1. CRC Press, Boca Raton, FL.
39. **Peña-Sandoval GR, Georgellis D.** 2010. The ArcB sensor kinase of *Escherichia coli* autophosphorylates by an intramolecular reaction. J. Bacteriol. **192:**1735-1739.
40. **Perrenoud A, Sauer U.** 2005. Impact of global transcriptional regulation by ArcA, ArcB, Cra, Crp, Cya, Fnr, and Mlc on glucose catabolism in *Escherichia coli*. J. Bacteriol. **187:**3171-3179.
41. **Rolfe MD, Ter Beek A, Graham AI, Trotter EW, Shahzad Asif HM, Sanguinetti G, Teixeira de Mattos MJ, Poole RK, Green J.** 2011. Transcript profiling and inference of *Escherichia coli* K-12 ArcA activity across the range of physiologically relevant oxygen concentrations. J. Biol. Chem. **286:**10147-10154.
42. **Ruiz JA, Fernández RO, Nikel PI, Méndez BS, Pettinari MJ.** 2006. *dye* (*arc*) Mutants: insights into an unexplained phenotype and its suppression by the synthesis of poly(3-hydroxybutyrate) in *Escherichia coli* recombinants. FEMS Microbiol. Lett. **258:**55-60.
43. **Salmon KA, Hung SP, Steffen NR, Krupp R, Baldi P, Hatfield GW, Gunsalus RP.** 2005. Global gene expression profiling in *Escherichia coli* K-12: effects of oxygen availability and ArcA. J. Biol. Chem. **280:**15084-15096.
44. **Sambrook J, Russell DW.** 2001. Molecular cloning: a laboratory manual, 3rd ed. Cold Spring Harbor Laboratory Press, Cold Spring Harbor, NY.

45. **Sánchez AM, Bennett GN, San KY.** 2006. Batch culture characterization and metabolic flux analysis of succinate-producing *Escherichia coli* strains. Metab. Eng. **8:**209-226.
46. **Sawers G.** 1993. Specific transcriptional requirements for positive regulation of the anaerobically inducible *pfl* operon by ArcA and FNR. Mol. Microbiol. **10:**737-747.
47. **Schwalbach MS, Keating DH, Tremaine M, Marner WD, Zhang Y, Bothfeld W, Higbee A, Grass JA, Cotten C, Reed JL, da Costa Sousa L, Jin M, Balan V, J. E, Dale B, Kiley PJ, Landick R.** 2012. Complex physiology and compound stress responses during fermentation of alkali-pretreated corn stover hydrolysate by an *Escherichia coli* ethanologen. Appl. Environ. Microbiol. **78:**3442-3457.
48. **Shalel-Levanon S, San KY, Bennett GN.** 2005. Effect of oxygen on the *Escherichia coli* ArcA and FNR regulation systems and metabolic responses. Biotechnol. Bioeng. **89:**556-564.
49. **Shalel-Levanon S, San KY, Bennett GN.** 2005. Effect of oxygen, and ArcA and FNR regulators on the expression of genes related to the electron transfer chain and the TCA cycle in *Escherichia coli*. Metab. Eng. **7:**364-374.
50. **Steiner P, Fussenegger M, Bailey JE, Sauer U.** 1998. Cloning and expression of the *Zymomonas mobilis* pyruvate kinase gene in *Escherichia coli*. Gene **220:**31-38.
51. **Stephanopoulos G.** 1999. Metabolic fluxes and metabolic engineering. Metab. Eng. **1:**1-11.
52. **Thakker C, Martínez I, San KY, Bennett GN.** 2012. Succinate production in *Escherichia coli*. Biotechnol. J. **7:**213-224.
53. **Tsai SP, Lee YH.** 1988. Application of metabolic pathway stoichiometry to statistical analysis of bioreactor measurement data. Biotechnol. Bioeng. **32:**713-715.
54. **Tseng CP, Albrecht J, Gunsalus RP.** 1996. Effect of microaerophilic cell growth conditions on expression of the aerobic (*cyoABCDE* and *cydAB*) and anaerobic (*narGHJI*, *frdABCD*, and *dmsABC*) respiratory pathway genes in *Escherichia coli*. J. Bacteriol. **178:**1094-1098.
55. **Varma A, Palsson BØ.** 1994. Stoichiometric flux balance models quantitatively predict growth and metabolic by-product secretion in wild-type *Escherichia coli* W3110. Appl. Environ. Microbiol. **60:**3724-3731.
56. **Veeger C, DerVartanian DV, Zeylemaker WP.** 1969. Succinate dehydrogenase. Methods Enzymol. **13:**81-90.

57. **Vickers CE, Klein-Marcuschamer D, Krömer JO.** 2012. Examining the feasibility of bulk commodity production in *Escherichia coli*. Biotechnol. Lett. **34:**585-596.

58. **Weitzman PDJ.** 1969. Citrate synthase from *Escherichia coli*. Methods Enzymol. **13:**22-26.

59. **Zhu J, Shalel-Levanon S, Bennett GN, San KY.** 2006. Effect of the global redox sensing/regulation networks on *Escherichia coli* and metabolic flux distribution based on C-13 labeling experiments. Metab. Eng. **8:**619-627.

FIGURE LEGENDS

FIG. 1 (A) Schematic representation of the ArcB protein. The different modules in the sensor protein are indicated with boxes, along with the amino acid coordinates they span. Individual amino acids relevant in the intramolecular phosphorelay that passes the phosphate residue among the different ArcB domains (which ultimately leads to phosphorylation of ArcA) are shown below the corresponding modules in the protein. Note that the elements in this outline are not drawn to scale. TM, transmembrane domain; LZ, leucine zipper. (B) Dye phenotype of the strains under study on toluidine blue O medium. Strains were firstly grown in LB medium under oxic conditions and adequate dilutions in cold saline were spotted onto the plates as previously described (9, 42). Plates were photographed after overnight incubation at 37°C, and representative colonies resulting from the 10^{-6} dilution are shown at a 13.4× magnification.

FIG. 2 Metabolic network used to study central catabolism of D-glucose in different *E. coli arcB* mutants under anoxic conditions. Fluxes within the network are codified as v_0 (which corresponds to the specific rate of D-glucose consumption) to v_{12}. Note that in this representation some biochemical reactions (*e.g.*, those generating biomass precursors from D-glucose-6-*P*) are lumped into a single flux in order to simplify the representation of the biochemical network. Enzymes that were assayed *in vitro* are highlighted in gray in the corresponding flux at which they are involved, and genes quantified at the transcriptional level are shown in a gray box beside their associated flux. The subscript *res* indicates accumulation of either residual pyruvate or formate in the culture medium. CoA, coenzyme A.

FIG. 3 Transcriptional analysis of relevant genes and *in vitro* enzymatic activity measurements during exponential growth of *E.* coli K1060 (wild-type strain) and its *arcB* mutant derivatives [GNB1061 ($ArcB^{268-520}$), GNB1062 ($ArcB^{177-640}$), and GNB1063 (Δ*arcB*)] in anoxic batch cultures developed in M9 minimal medium with 3% (wt/vol) D-glucose as the carbon source. (A) Results from quantitative RT-PCR analysis in the mutant strains are normalized to the corresponding transcript levels in *E. coli* K1060, and represent the mean value ± standard deviation of sextuplicate measurements from at least three independent cultures. (B) Results from determinations of specific enzymatic activities represent the mean value ± standard deviation of triplicate measurements from at least two independent cultures. Note that the activity of

pyruvate kinase (PykAF) is separately represented as the corresponding values were much higher than those obtained for the rest of the enzymes assayed. Sp, specific.

699 **TABLE 1** *E. coli* strains, oligonucleotides, and plasmids used in this study.

700

Strain, oligonucleotide, or plasmid	Relevant characteristics or sequence (5'→3')	Source or reference
E. coli		
K1060[a]	Considered wild-type in this study; F⁻ *fadE62 lacI60 tyrT58*(AS) *fabB5 mel-1*	(36)
GNB1061	Same as K1060, but ArcB$^{268\text{-}520}$; confined deletion between 802-1560 nt of *arcB*	This study
GNB1062	Same as K1060, but ArcB$^{177\text{-}640}$; confined deletion between 529-1920 nt of *arcB*	This study
GNB1063	Same as K1060, but Δ*arcB*	This study
Oligonucleotide[b]		
ΔPAS-F	TCC TTG ATG CTT CAC CCG ACC TGG TTT TTT ATC GTA ACG AAG ATA AAG AG**G TGT AGG CTG GAG CTG CTT C**	This study
ΔD1-R	TCT TCT GTC GTC ACC GTA CTC TCC TCA TCA TCC TGG GTA TCC CAG AAT TT**C ATA TGA ATA TCC TCC TTA G**	This study
ΔH1-F	ACC GCG TGG GTA AAC GTC ACG GTT TGA TGG GCT TTG GTC GCG ACA TTA CC**G TGT AGG CTG GAG CTG CTT C**	This study
ΔH1-R	TTC AGT TCA ATG TCT TCC ACC AGC AGC ACA TTC AGC GCC GGT AAA GGC AT**C ATA TGA ATA TCC TCC TTA G**	This study
Δ*arcB*-F	AAC GTA ACT GTC AGA ATT GGG TAT TAT TGG GGC AGG TTG TCG TGA AGG AA**G TGT AGG CGT GAG CTG CTT C**	This study
Δ*arcB*-R	ATA ATA ATT TAC GGC CGA GCC AAG ATT TCC CTG GTG TTG GCG CAG TAT TC**C ATA TGA ATA TCC TCC TTA G**	This study
arcB1-C-F	GGG TAT TAT TGG GGC AGG TT	This study
arcB1-C-R	GTC TAG CCG GGG TCA TTT TT	This study
arcB2-C-F	AAT GAT TCG CCA TAC GCC AC	This study

arcB2-C-R	GTG CTG TGC CCT TGT AAC TC	This study
PDH-C-F	GAG CAA CTG GAG GAG TCA CG	This study
PAS-C-R	GCA AGG AAG CTG GTG AAA TC	This study
H1-C-R	GGT GAT CAG CTT CGG TCC TA	This study
D1-C-R	CGG AAG GTC AGG AGA CTG AA	This study
rrsA-RT-F	AGG CCT TCG GGT TGT AAA GT	This study
rrsA-RT-R	ATT CCG ATT AAC GCT TGC AC	This study
pfkA-RT-F	GGT GCC TTA CGA CCG TAT TC	This study
pfkA-RT-R	GGA CGC TTC ATG TTT TCG AT	This study
ldhA-RT-F	AGT CCG TGT TCC AGC CTA TG	This study
ldhA-RT-R	CGG TCA GAC CTT CCA GAG AG	This study
pflB-RT-F	GCG AAA TAC GGC TAC GAC AT	This study
pflB-RT-R	CAT CCA GGA AGG TGG AGG TA	This study
ackA-RT-F	CGT TGA CGC AAT CAA CAA AC	This study
ackA-RT-R	GGT GGC AGT AAA CG TCC ATT	This study
adhE-RT-F	CTG GCA GGC TTC TCT GTA CC	This study
adhE-RT-R	TAC CGC GTC TTC GAA ATC TT	This study
frdA-RT-F	CGA TAA GAC CGG CTT CCA TA	This study
frdA-RT-R	CCT TCC ATC ATG TTC ATT GCT	This study
fdhF-RT-F	AAA AAG TCG TCA CGG TTT GC	This study
fdhF-RT-R	TTC GCG CAG GCG AGT TTT	This study
arcA-RT-F	TGT TTT CGA AGC GAC AGA TG	This study
arcA-RT-R	GAA CAT CAA CGC AAC ATT CG	This study
Plasmid		
pKD46	Vector containing the λ-Red (γ, β, and *exo*) recombination functions under control of the P_{araB} promoter; *oriR101*, *repA101*(Ts), Ap^r	(12)
pKD4	Vector used as template for amplification of *FRT-aphA-FRT*; *oriR6Kγ*, Ap^r Km^r	(12)

pCP20	Vector expressing the *FLP* recombinase from *Saccharomyces cerevisiae*; λ *c*I857 λ P_R *FLP repA*(Ts), Ap^r Cm^r	(10)

[a] Strain obtained through the *E. coli* Genetic Stock Center, University of Yale, CT.

[b] Sequences with homology to *FRT-aphA-FRT* in the template plasmid pKD4 are shown in boldface. Oligonucleotides used for deletions are preceded by the symbol Δ, and those used to check deletions are followed by the letter C. Oligonucleotides used for quantitative RT-PCR experiments are codified according to *target gene*-RT-F/R.

708 **TABLE 2** Fermentation and growth parameters[a] for 24-h anoxic batch cultures in M9 minimal
709 medium with 3% (wt/vol) D-glucose as the carbon source.
710

E. coli strain	Relevant characteristics	Biomass ($g \cdot liter^{-1}$)	μ_{max}[b] (h^{-1})	Sp rate of D-glucose consumption[b] ($mmol \cdot g^{-1} \cdot h^{-1}$)	$Y_{X/S}$ ($mg \cdot g^{-1}$)
K1060	Wild-type strain	0.65 ± 0.08	0.34 ± 0.02	7.22 ± 0.05	79 ± 2
GNB1061	$ArcB^{268-520}$	0.43 ± 0.04	0.27 ± 0.03	6.07 ± 0.04	54 ± 2
GNB1062	$ArcB^{177-640}$	0.26 ± 0.03	0.16 ± 0.01	5.31 ± 0.08	27 ± 1
GNB1063	Δ*arcB*	0.18 ± 0.02	0.11 ± 0.02	4.85 ± 0.06	21 ± 3

711
712 [a] Reported results represent the mean value ± standard deviation of triplicate measurements from at least
713 two independent cultures.
714 [b] The specific growth rate and the specific rate of D-glucose consumption were determined during balanced
715 growth.
716

717 **TABLE 3** Redox parameters[a] for 24-h anoxic batch cultures in M9 minimal medium with 3% (wt/vol)
718 D-glucose as the carbon source.
719

E. coli strain	Relevant characteristics	Intracellular content ($\mu mol \cdot g^{-1}$) of:		NADH/NAD^+ ratio ($mol \cdot mol^{-1}$)	Ethanol/acetate ratio ($mol \cdot mol^{-1}$)
		NADH	NAD^+		
K1060	Wild-type strain	2.03 ± 0.09	3.96 ± 0.07	0.51 ± 0.05	0.53 ± 0.05
GNB1061	$ArcB^{268-520}$	2.14 ± 0.08	3.45 ± 0.21	0.62 ± 0.04	0.63 ± 0.03
GNB1062	$ArcB^{177-640}$	2.91 ± 0.12	3.93 ± 0.15	0.74 ± 0.08	0.74 ± 0.03
GNB1063	Δ*arcB*	2.61 ± 0.05	3.02 ± 0.09	0.86 ± 0.06	0.81 ± 0.02

720
721 [a] Reported results represent the mean value ± standard deviation of duplicate measurements from at least
722 two independent cultures.
723

TABLE 4 Metabolic flux distribution in anoxic batch cultures of *E. coli* K1060 and its *arcB* mutant derivatives during balanced growth in M9 minimal medium with 3% (wt/vol) D-glucose as the carbon source.

Flux	Flux to:	Relative flux[a] for *E. coli*:			
		K1060 (wild-type strain)	GNB1061 ($ArcB^{268-520}$)	GNB1062 ($ArcB^{177-640}$)	GNB1063 (Δ*arcB*)
v_0[b]	D-Glucose-6-*P*	100	100	100	100
v_1	Biomass	21.1 ± 0.9	19.9 ± 0.2	16.7 ± 0.4	13.8 ± 0.6
v_2	D-Glyceraldehyde-3-*P*	78.9 ± 1.3	80.1 ± 1.4	83.3 ± 1.5	86.2 ± 1.9
v_3	*P-enol*-pyruvate	157.8 ± 2.5	160.3 ± 2.9	166.7 ± 1.8	172.4 ± 3.6
v_4	Pyruvate	152.9 ± 0.8	153.1 ± 0.9	156.5 ± 0.9	159.2 ± 0.4
v_5	Succinate	4.8 ± 0.5	7.2 ± 0.6	10.2 ± 0.7	13.2 ± 0.3
v_6	Residual pyruvate	1.7 ± 0.3	1.8 ± 0.1	0.0 ± 0.1	0.0 ± 0.2
v_7	D-Lactate	3.2 ± 0.4	4.6 ± 0.5	6.6 ± 0.4	8.5 ± 0.1
v_8	Acetyl-CoA	148.1 ± 0.7	148.4 ± 0.3	149.9 ± 0.9	150.7 ± 0.9
v_9	Residual formate	79.5 ± 0.9	86.7 ± 1.1	91.3 ± 0.7	91.5 ± 1.2
v_{10}	H_2	68.6 ± 1.2	61.8 ± 0.9	58.6 ± 1.4	59.2 ± 0.6
v_{11}	Ethanol	65.9 ± 0.8	68.7 ± 0.4	76.3 ± 0.5	81.6 ± 0.3
v_{12}	Acetate	82.1 ± 0.7	79.7 ± 0.7	73.6 ± 0.2	69.1 ± 0.2
	Carbon balance[c]	0.93 ± 0.04	0.96 ± 0.02	0.91 ± 0.12	0.92 ± 0.09

[a] The relative flux values were normalized to the specific rate of D-glucose consumption in each strain (v_0), and the reported results represent the mean value ± 90% confidence intervals calculated using triplicate measurements of extracellular fluxes in at least two independent cultures. Fluxes were codified according to the biochemical reactions as shown in Fig. 2.

[b] Absolute flux values for v_0 are as shown in Table 2.

[c] Carbon balances were calculated from experimental fluxes to extracellular metabolites, inferred rate of CO_2 evolution, and biomass generation. The reported results represent the mean value ± standard deviation calculated from the flux values within the metabolic network.

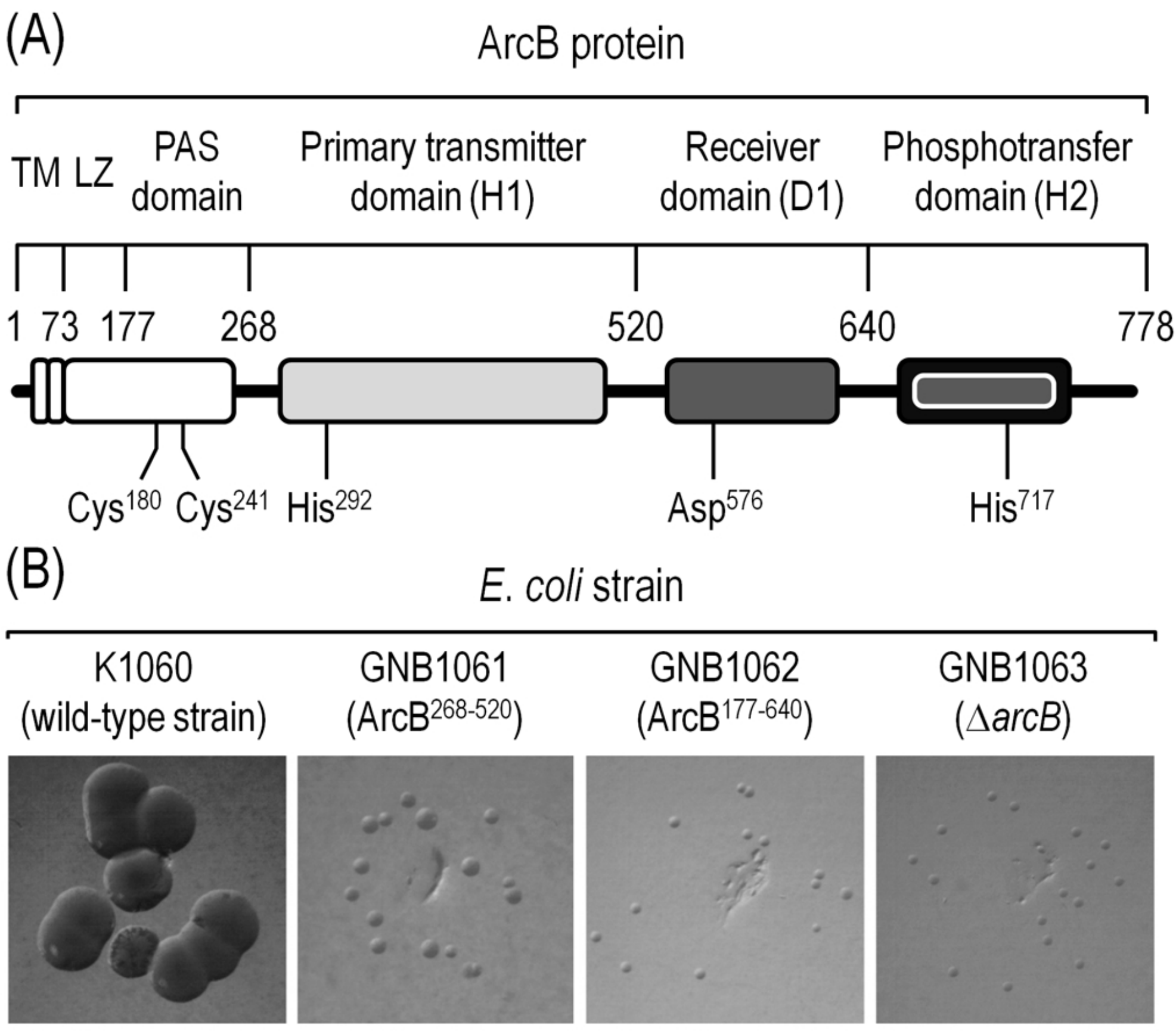
(A)
ArcB protein
TM LZ
PAS domain
Primary transmitter domain (H1)
Receiver domain (D1)
Phosphotransfer domain (H2)
1 73 177 268 520 640 778
Cys180 Cys241 His292 Asp576 His717
(B)
E. coli strain
K1060 (wild-type strain)
GNB1061 (ArcB268-520)
GNB1062 (ArcB177-640)
GNB1063 (ΔarcB)

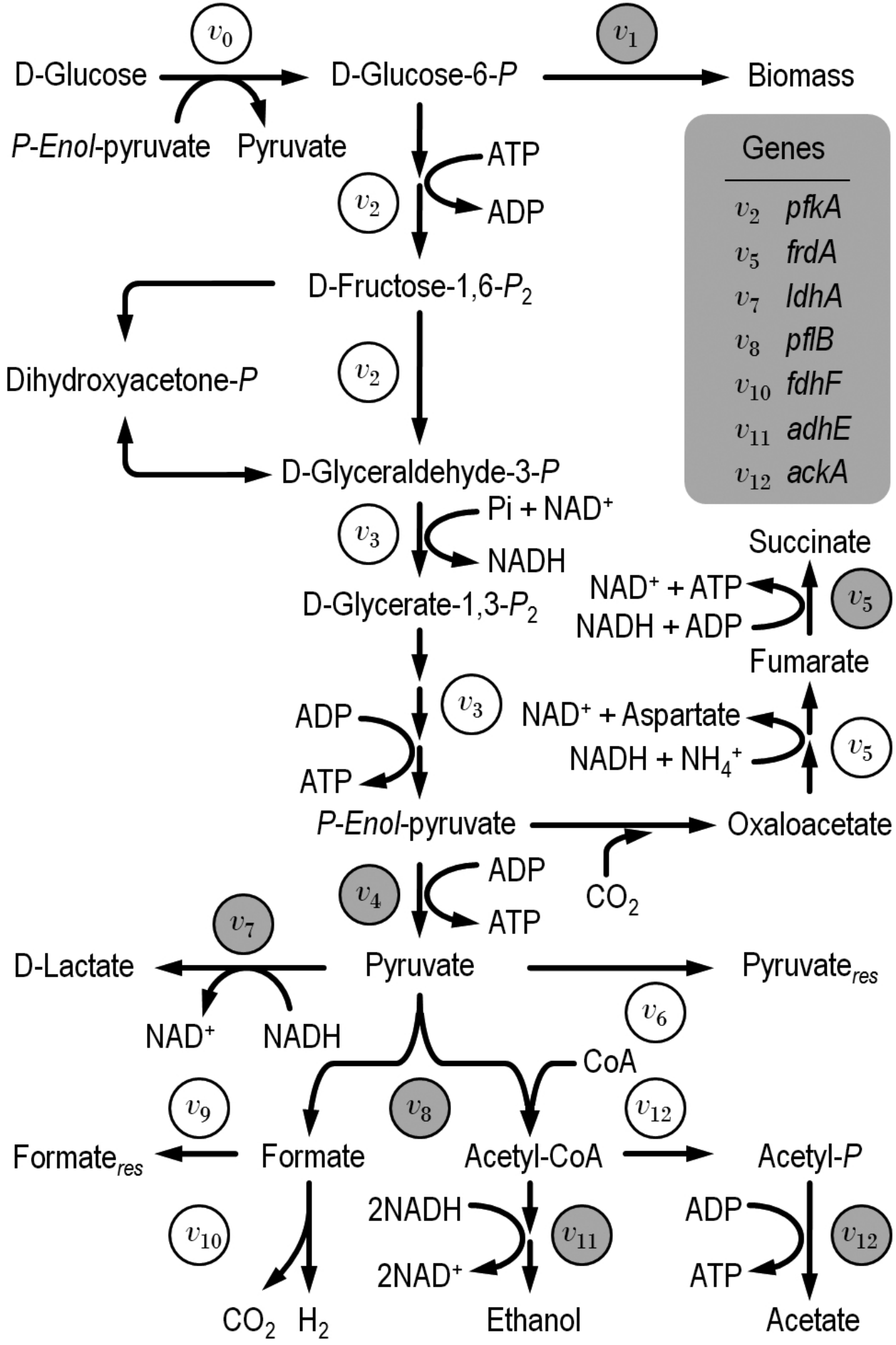
v_0
D-Glucose
P-Enol-pyruvate
Pyruvate
v_1
D-Glucose-6-P
Biomass
ATP
ADP
v_2
D-Fructose-1,6-P2
Dihydroxyacetone-P
v_2
D-Glyceraldehyde-3-P
Pi + NAD+
NADH
v_3
D-Glycerate-1,3-P2
ADP
ATP
v_3
P-Enol-pyruvate
Succinate
NAD+ + ATP
NADH + ADP
v_5
Fumarate
NAD+ + Aspartate
NADH + NH4+
v_5
Oxaloacetate
CO2
ADP
ATP
v_4
v_7
D-Lactate
NAD+
NADH
Pyruvate
Pyruvate_res
v_6
CoA
v_9
v_8
v_{12}
Formate_res
Formate
Acetyl-CoA
Acetyl-P
v_{10}
2NADH
2NAD+
v_{11}
ADP
ATP
v_{12}
CO2
H2
Ethanol
Acetate
Genes
v_2 pfkA
v_5 frdA
v_7 ldhA
v_8 pflB
v_{10} fdhF
v_{11} adhE
v_{12} ackA

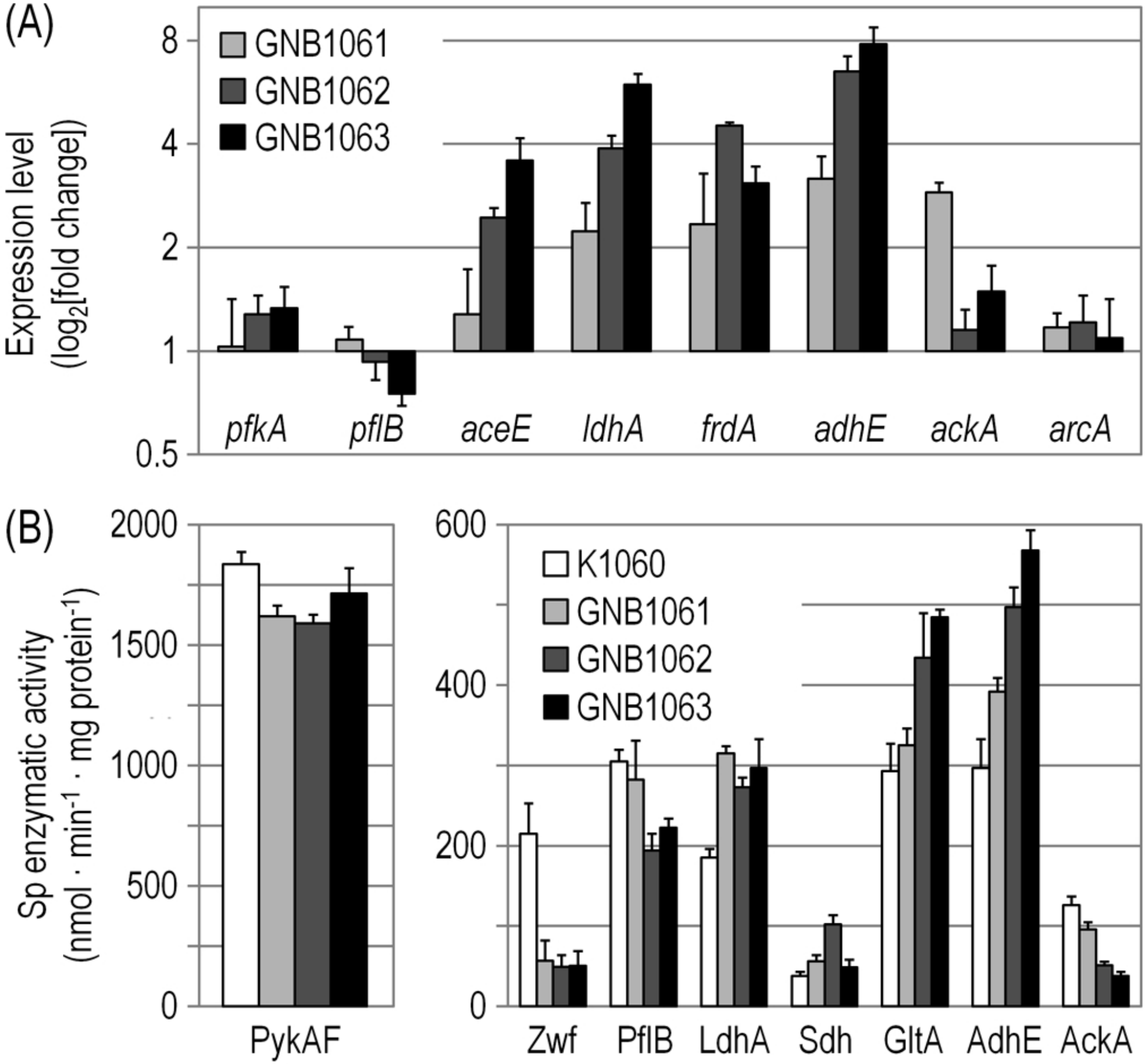
(A)
GNB1061
GNB1062
GNB1063
Expression level
(log2[fold change])
8
4
2
1
0.5
pfkA
pflB
aceE
ldhA
frdA
adhE
ackA
arcA
(B)
Sp enzymatic activity
(nmol · min-1 · mg protein-1)
2000
1500
1000
500
0
PykAF
600
400
200
0
K1060
GNB1061
GNB1062
GNB1063
Zwf
PflB
LdhA
Sdh
GltA
AdhE
AckA